Molecular-Based Virial Coefficients of CO_2-H_2O Mixtures

Andrew J. Schultz[1], David A. Kofke[1]*, and Allan H. Harvey[2]

[1]*Department of Chemical and Biological Engineering*

University at Buffalo, The State University of New York, Buffalo, NY, 14260, USA

[2]*Applied Chemicals and Materials Division*

National Institute of Standards and Technology, 325 Broadway, Boulder, Colorado 80305, USA

Abstract

We report second and third virial coefficients for the system CO_2-H_2O, calculated via cluster integrals using quantitative molecular models taken from the literature. Considered models include (1) fits to highly accurate *ab initio* calculations of the potential energy surfaces, and (2) semi-empirical Gaussian Charge Polarizable Models (GCPM). Three-body effects are found to be essential for obtaining quantitative results. Good agreement with experiment is obtained for the pure- component coefficients, and for the cross second virial coefficient. For the two cross third virial coefficients, the few experimental data available do not agree well with the calculations; it is not clear whether this is due to problems with the data or deficiencies in the three-body potentials. The uncertain state of the experimental data, and the relative mutual

*electronic mail: kofke@buffalo.edu

consistency of values computed from *ab initio* and GCPM models, suggest that calculated mixture third virial coefficients could be more accurate than values from experiment.

Introduction

As processes for carbon capture and sequestration (CCS) are evaluated and developed, knowledge of the thermodynamic properties of mixtures containing CO_2 is increasingly important.[1] Mixtures containing water are present throughout the processes. One area of particular interest is in pipeline transportation, where the water content of the compressed CO_2 must be lowered in order to avoid condensation that can lead to corrosion. Previous surveys[2,3] indicated that existing data for the dew point of water in compressed CO_2 are inconsistent and scattered at typical pipeline conditions. Mixtures containing CO_2 and H_2O at moderate pressures also arise in advanced power cycles that facilitate carbon capture.[4–6]

For the vapor phase in such systems, it is often convenient to formulate the thermodynamics in terms of the virial equation of state (VEOS),[7] where deviations from ideal-gas behavior are expressed as a power series in molar density ρ or pressure P. The series in density is most often used:

$$\frac{P}{RT} = \rho + \sum_{n=2}^{\infty} B_n \rho^n, \tag{1}$$

where R is the gas constant, T is the temperature, and B_n is the n^{th}-order virial coefficient. The expansion is often truncated after the second or third virial coefficients, which for a binary mixture are given, respectively, as a function of mole fractions y_i as

$$B_2 = B_{20}y_1^2 + 2B_{11}y_1y_2 + B_{02}y_2^2 \tag{2}$$

$$B_3 = B_{30}y_1^3 + 3B_{21}y_1^2y_2 + 3B_{12}y_1y_2^2 + B_{03}y_2^3, \tag{3}$$

where the coefficients B_{ij} are functions only of temperature. Values for these coefficients can be obtained by appropriate analysis of experimental $PVTy$ data or, increasingly so, by calculations based on accurate molecular models. Indeed, the VEOS is unique among engineering equations of state in its ability to determine its parameters rigorously from molecular considerations. Our focus in this work is on such an approach to developing a model for CO_2(1)-H_2O(2) gas mixtures, based on molecular models that are accurate at low density, particularly those that have been formulated using data obtained only by *ab initio* computational chemistry methods.

Virial coefficients computed from molecular models are useful in several ways. First, they can by themselves provide an equation of state (EOS) suitable for practical applications. For example, we used them to describe non-idealities in the gas phase to improve interpretation of gas-saturation measurements of the vapor pressure of low-volatile compounds.[8] Such an application is particularly well suited for

computed virial coefficients, because experimental $PVTy$ data for these systems is, by definition, difficult to obtain. Second, calculated virial coefficients provide boundary conditions to be satisfied when fitting parameters for other types of equations of state. This synthesis reduces empiricism while enforcing appropriate low-density behavior on the EOS. Alternatively, such a hybrid can be viewed as a kind of resummation of the virial series, producing an approximant that is applicable beyond the region where the virial series to a given order is converged. This approach is particularly powerful if the hybrid form satisfies known behavior in another region of state space. We have demonstrated this idea in formulating equations of state for the full family of soft-sphere models,[9] each one accurate over all of its respective fluid-phase region; we demonstrated it again in forming an approximant based on universal scaling near the vapor-liquid critical region, yielding a model isotherm that is accurate at all densities up to the critical point.[10] Finally, computed virial coefficients can be used in conjunction with experimental data, providing leverage that allows more accurate and precise values of the virial coefficients to be extracted from the data. This was first done by Moldover and McLinden,[11] who evaluated B_4 for helium from experimental data using published values of B_2 and B_3 that were computed from an *ab initio*-based molecular model. Subsequently, Shaul et al.[12] introduced computed values of B_5 to generate even better estimates of B_4 from the

same experimental data. These B_5-enhanced values from experiment were shown to be much more consistent with computed B_4 values, in comparison to those derived using just B_2 and B_3.

Extension of this undertaking to mixtures becomes significantly more complicated, owing to the increasing variety of interactions that require consideration. With respect to mixtures of CO_2 and H_2O, the second virial coefficient is known accurately from experiment for pure CO_2 (B_{20})[13] and pure H_2O (B_{02}),[14] but full treatment of the mixture requires also the coefficient B_{11}, which calls for extensive data for the CO_2-H_2O mixtures. Such data are not as plentiful as for the pure species, and it is here that calculation from a molecular model can be most useful. This coefficient is based on the interaction between a CO_2 and an H_2O molecule. Wheatley and Harvey[2] developed a high-quality CO_2-H_2O pair potential and used it to calculate B_{11} over a wide range of temperatures, extending both below and above the range of available experimental data. Their values were confirmed in the temperature range $10\,^{\circ}\mathrm{C} \leq t \leq 80\,^{\circ}\mathrm{C}$ by the recent high-accuracy dew-point experiments of Meyer and Harvey.[3] Given this characterization of B_{11} and the reliable experimental values of B_{20} and B_{02}, we can say that the thermodynamics of CO_2-H_2O mixtures are known with good accuracy at the second virial level.

However, in some important cases, the second virial level is not sufficient. Meyer

and Harvey[3] found that third virial coefficients were necessary to describe their dew-point data at pressures above approximately 2 MPa; this is well below expected pipeline pressures, which might reach 10 MPa or more. Unfortunately, their data were not precise enough to determine cross third virial coefficients with much certainty; the coefficient B_{21} was determined with large uncertainties while B_{12} was estimated in a very approximate way. Another source of experimental third virial coefficients[15] has large uncertainties and does not cover temperatures as low as those present in pipelines.

So we again have a case where virial coefficients computed from a molecular model can potentially fill a void in the base of experimental data. There are four coefficients at the third-virial level, including the two pure-fluid coefficients, B_{30} and B_{03}, and two cross coefficients, B_{21} and B_{12}. If the interactions are pairwise additive, then all of these coefficients can be computed with the same 2-body potentials used to compute B_{20}, B_{11}, and B_{02}. However, 3-body effects are not negligible at the significance level of interest to this work, so some means is needed to account for them. We will discuss this and other molecular modeling issues in the next section. Following that, we describe the methods used to compute the virial coefficients from the CO_2-H_2O molecular models. We then present and discuss results, and in the final section provide some concluding remarks.

Molecular Modeling

The potential energy U of interaction of N molecules is conventionally expressed as a series:

$$U = U_2 + U_3 + U_4 + ..., \tag{4}$$

where U_2 is the sum of the energy of each pair of molecules, U_3 is the sum of the energy of each set of three molecules in excess of its pairwise sum, and so on for groups of four or more molecules in U_4, U_5, etc. Full consideration of the energy would also include a sum of one-body contributions that characterize the change in intramolecular energy caused by distortion of each molecule as it interacts with the others; such effects will not be included in this work. The n^{th} virial coefficient is given as an integral over the positions and orientations of n molecules, and hence requires knowledge of the terms in Eq. (4) only up to U_n. Accordingly, comparison of a calculated $B_2(T)$ to experiment can be used to test the accuracy of U_2, $B_3(T)$ can test U_3, and so on.

Although the second virial coefficients for H_2O and CO_2 are well characterized from experiment, we still need to consider the performance of pair potentials in describing them, because pair interactions form the starting point for calculations of the third virial coefficient. There now exist countless pair potentials that have been developed for water. Many of these are fixed-charge models that have been

formulated to describe the liquid phase, and these have been shown to provide a very poor description of the virial coefficients.[16] Polarizable models perform much better in this respect, and in particular the Gaussian charge polarizable model (GCPM) for water[17] provides an excellent description of B_2 and B_3.[18,19] There is also a GCPM for CO_2,[20] which was fit in part using experimental virial-coefficient data. We will examine GCPM formulations in this work, but they are not the most desirable type of molecular model for our purposes: while they are parameterized in part using *ab initio* calculations (for geometry and electrostatics), their formulation is also based on experimental data for the condensed phase. This means that some features of the intermolecular interactions (e.g., exchange repulsion, nuclear quantum effects) are lumped in as part of their parameterization, and are not handled specifically. This may make the models less suited to describe behavior with unlike molecules.

We therefore turn to models that are based on *ab initio* calculations. Formulation of these models begins with high-level *ab initio* calculations performed for a large set of configurations (each involving n molecules when computing U_n) that are relevant to the behavior of the system. This sample of the potential-energy surface is then fit to a physically meaningful form, constructed from terms that describe the expected behavior of various contributions to the intermolecular energy. Thus, most of the models start with an exp-6 form to capture repulsion and 2-body dispersion, and add

other terms as appropriate to capture electrostatics, induction, higher-order dispersion, exchange, and so on; massless interaction sites may be added to better describe the charge distribution or anisotropic polarizability. A fitting procedure is then applied to specify various adjustable parameters that appear in the model. Three-body potentials are developed in a similar manner, and typically will account for 3-body dispersion, induction, and exchange in separate contributions. Notably, for water, it has been shown[21] that simple polarization effects (such as those accounted for by a GCPM), capture only about 50% of the total 3-body contribution in the condensed phase.

The task of generating quantitatively useful multi-body potentials from *ab initio* methods is difficult, even for small molecules such as H_2O and CO_2. The H_2O trimer has 21 degrees of freedom, and to generate just 2 points per dimension would require more than two million configurations. This burden is considerably reduced by working with rigid monomers, which then form a 12-dimensional space of configurations. The state of the art now is such that it is feasible to perform accurate first-principles energy calculations for tens of thousands of configurations, which supports only about 2.5 configurations per dimension. This puts particular importance on the choice of the functional form for the model, and selection of the most relevant molecular configurations to fit its parameters.

For H_2O-H_2O pair interactions, we adopt the rigid-monomer "CCpol2" model of Góra et al.,[22] which employs 8 symmetry-unique interaction sites (25 sites in all) per water monomer, and is fit to *ab initio* energies for 3216 configurations (averaging 3.8 per dimension). Interactions are functions of site-site distances, r, and include an exponential repulsion multiplying a 4-term polynomial in r, point-charge electrostatics, dispersion, and various damping factors; not all interaction terms apply to all site-site pairs. Altogether it has a total of 278 parameters, including site coordinates, partial charges, damping coefficients, and other model parameters. Added to this is an induction contribution, which is the 2-body case of a more general n-body polarization model. Induction is described using three polarization centers, one located on each atomic site, with polarizabilities determined directly from *ab initio* calculations on the monomer. The electrostatic interactions giving rise to polarization are damped, and this introduces two more parameters, which were fitted with consideration to 3- and 4-body non-additive energies. The model was tested by Góra et al. via examination of the energetics of the water trimer, hexamer, and 24-mer, but they did not use it to compute virial coefficients.

For CO_2-CO_2, we employ the 2-body rigid-monomer potential proposed by Hellmann,[23] which is based on a fit of 1229 *ab initio* interaction energies (5.9 points per dimension). The model employs four symmetry-unique sites (seven sites in all)

per CO_2 molecule, and has 54 independent parameters for fitting (accounting for constraints imposed on the fit to satisfy known conditions, such as the molecular quadrupole moment). It includes exponential repulsion, damped dispersion, and point-charge electrostatics. Hellmann computed values of the second virial coefficient based on his model, and showed good agreement with available experimental data. He then applied a small adjustment to the treatment of the *ab initio* data and refit the model, further improving the comparison to experiment; this "V_B" potential is the one used here.

For the cross interaction, we turn to the H_2O-CO_2 pair potential proposed by Wheatley and Harvey,[2] mentioned above. This is based on *ab initio* energies for 5285 pair configurations (5.6 points per dimension), fit to a 110-parameter function that sums various products and powers of internuclear distances; thus, each molecule is represented by three interaction sites. Wheatley and Harvey's calculation of B_{11} gives results that are consistent with what is known experimentally.

We describe now the treatment of 3-body interactions, U_3 in Eq. (4). Four effects are considered relevant: (1) 3-body induction is concerned with how the electrostatic interaction of two molecules distorts their charge distribution, which affects how each interacts with a third molecule; (2) 3-body dispersion describes how instantaneous fluctuations in the electron distribution of neighboring atoms couple to generate a

contribution to the intermolecular energy; (3) the exchange interaction is a purely quantum-mechanical effect that results from the symmetry of the electronic wave function, and in the present context relates to exchange of electrons on different molecules. 3-body exchange is a short-range effect, but in addition, (4) exchange between two molecules can alter their electronic structure, thereby producing an induction-like effect that alters how each will interact with a third molecule. This "exchange-induction" interaction can be longer ranged.

In the absence of a 3-body potential developed for a specific set of three CO_2 and/or H_2O molecules, we apply general formulations for induction and dispersion. Induction is modeled by adding a single isotropic polarization site on each molecule, and rather than converge the electric field, we use the direct, approximate form given by Oakley and Wheatley,[24]

$$U_{3,\mathrm{ind}} = -\sum_{a,b,c} q_a q_c \alpha_b r_{ab}^{-2} r_{bc}^{-2} \cos\theta_b. \tag{5}$$

The charges (q) and polarizabilities (α) here have values and locations as specified for the homogeneous potentials, i.e., for H_2O, those given by CCpol2,[22] and for CO_2, by Hellmann.[23] The sum is over these interaction sites, labeled a, b, c, each on a different molecule, with all uniquely-contributing permutations (i.e., three specific interaction sites will contribute three terms, such that each site plays the role of b exactly once for that triple). Then θ_b is the angle formed by sites abc, and r_{ij} is the

intersite distance.

Three-body dispersion is treated using the Axilrod-Teller triple-dipole form:[25–27]

$$U_{3,\mathrm{disp}} = \nu_{abc}\,(1 + 3\cos\theta_a \cos\theta_b \cos\theta_c)\, r_{ab}^{-3} r_{ac}^{-3} r_{bc}^{-3}, \tag{6}$$

with one isotropic interaction site per molecule; parameters ν_{abc} are based on the known polarizability α and ionization potential V of CO_2 ($\alpha = 2.913 \times 10^{-24}$ cm^3,[27] $V = 13.7$ eV[7] (1 eV $\approx 1.602 \times 10^{-19}$ J)) and H_2O ($\alpha = 1.444 \times 10^{-24}$ cm^3,[17,28] $V = 12.6$ eV[7]); the necessary relation is given by Axilrod.[26] We do not attempt to model multibody exchange or exchange-induction in the general case.

For the case of the H_2O trimer, Góra et al.[22] provide a fit to 76,208 energies (2.6 per dimension). This "CCpol23" potential was developed in conjunction with the CCpol2 dimer model described above. Multibody induction is captured with the same polarization model used for the dimer. Exchange-induction is modeled via an induced quadrupole moment: four point charges—with magnitude decaying exponentially with separation—are placed on the line joining the centers of two molecules, and allowed to interact with the permanent charges on a third molecule. The remaining 3-body exchange and dispersion contributions are modeled together with a sum over triplets of interaction sites (each from a different molecule), with each term in the sum depending on the three interaction-site distances. There are 6 symmetry-unique interaction sites (17 sites in all) on each molecule, all coinciding

with sites used for the pair interaction (but not including all pair sites). Altogether there are 471 independent parameters in this part of the model, in addition to 2 other parameters associated with the exchange-induction component. In all the trimer configurations used for the fit, the molecules were separated by no more than 0.7 nm, so the energy of any configuration having water molecules separated by more than this represents an extrapolation of the fit, and is not likely to be reliable (we indeed find anomalous and almost certainly incorrect behavior for separations of 2 nm or so). Accordingly, we set the 3-body potential to zero when any pair is separated by more than 0.7 nm.

Hellmann did not develop a 3-body potential for the CO_2 trimer to accompany his pair potential. Yu and Schmidt[29] developed a 3-body model to supplement a 2-body potential formulated by them previously (we prefer the Hellmann 2-body potential because it is based on higher-level *ab initio* calculations). The Yu-Schmidt 3-body potential includes dispersion, induction, and exchange, and the model is fit in part to experimental B_3. We do not use this model for our calculations, but we do include the results reported by Yu and Schmidt in our comparisons.

There are no published 3-body potentials for mixtures of CO_2 and H_2O molecules, which are required for B_{12} and B_{21}. For these cases, we use the forms given by Eqs. (5) and (6).

To provide an independent alternative representation of the CO_2-H_2O system, we also examined GCPM formulations for these molecules. Such models have been proposed for H_2O[17] and for CO_2,[20] but not their mixtures. For the present study, we extended these treatments to the cross CO_2-H_2O interactions. The hybrid potential developed in this way was considered by Persson,[20] but not in the context of virial coefficients. Before describing our extension, we will review the models as they were originally developed for the pure species. Both models are rigid, and employ an atom-centered exp-6 representation of repulsion and 2-body dispersion,

$$u(r) = \frac{\varepsilon}{1-6/\gamma}\left[\frac{6}{\gamma}\exp\left\{\gamma\left(1-\frac{r}{\sigma}\right)\right\} - \left(\frac{\sigma}{r}\right)^6\right], \tag{7}$$

where the parameters σ, ϵ, and γ in Eq. (7) are in general different for different types of interaction-site pairs. Both models use smeared Gaussian charges to describe their permanent (lone-molecule) electron distribution, and both add to this a polarizable point dipole, which is induced by interactions with the permanent and induced dipoles on surrounding molecules; all dipoles and electric fields are solved self-consistently for each configuration. The CO_2 model also has an Axilrod-Teller contribution, with a single anisotropic dispersion site located on the C atom. For GCPM water, parameters for the width of the Gaussian-charge distribution, the exp-6 contribution, and the location of the negative charge were determined from fits to experimental data for liquid water and vapor-liquid coexistence.[17] For CO_2, param-

eters were fit to experimental data for the second virial coefficient $B_2(T)$, and the Axilrod-Teller parameter was selected to reproduce experimental data for $B_3(T)$.[20]

From this starting point, we set up a hybrid GCPM for CO_2-H_2O as follows. Electrostatic and dipole-polarization interactions for heterogeneous sets of molecules are treated exactly in the same manner as they are for the pure substances, with the same charge distributions and polarizabilities. For the exp-6 contribution, we start with the standard combining rules (which are also used in the CO_2 potential for the C-O interaction):[20]

$$\begin{aligned} \varepsilon_{\alpha\beta} &= \frac{2\varepsilon_{\alpha\alpha}\varepsilon_{\beta\beta}}{\varepsilon_{\alpha\alpha}+\varepsilon_{\beta\beta}} \\ \sigma_{\alpha\beta} &= \frac{1}{2}\left(\sigma_{\alpha\alpha}+\sigma_{\beta\beta}\right) \\ \gamma_{\alpha\beta} &= \frac{1}{2}\left(\gamma_{\alpha\alpha}+\gamma_{\beta\beta}\right) \end{aligned} \tag{8}$$

We find that the virial coefficient $B_{11}(T)$ given by these nominal combining rules does not agree well with experiment (as shown below), so we multiplied the combining-rule values by corresponding parameters k_σ, k_ϵ, and k_γ, using the same multipliers for the H_2O oxygen in its interactions with both the CO_2 carbon and oxygens. A good fit to the experimental $B_{11}(T)$ was obtained with $k_\sigma = 0.99$, $k_\epsilon = 1.10$, and $k_\gamma = 0.96$. GCPM water does not have a 3-body dispersion term, so we considered adding an Axilrod-Teller contribution to it, to improve compatibility with the GCPM CO_2 potential. We found, however, that the effect from such a term was small and

not generally helpful, so we did not include 3-body dispersion in the model.

Our aim in formulating the GCPM for CO_2-H_2O is not to show it can yield agreement with experimental $B_{11}(T)$ values, but rather to provide the best basis possible within the GCPM framework to understand the third virial coefficients B_{12} and B_{21}, for which experimental data are not so reliable.

Calculation of Virial Coefficients

The second and third virial coefficients are given in terms of the following integrals, in which molecule 1 is placed at the origin:

$$B_{ij} = -\frac{1}{2}\int \langle f_{12}\rangle_{\Omega_1\Omega_2} d\mathbf{r}_2 \qquad i+j=2 \tag{9}$$

$$B_{ij} = B_{ij}^{(\text{pair})} + B_{ij}^{(\text{non-pair})} \qquad i+j=3 \tag{10}$$

$$B_{ij}^{(\text{pair})} = -\frac{1}{3}\int \langle f_{12} f_{13} f_{23}\rangle_{\Omega_1\Omega_2\Omega_3} d\mathbf{r}_2 d\mathbf{r}_3$$

$$B_{ij}^{(\text{non-pair})} = -\frac{1}{3}\int \left\langle e^{-\beta U_2}\left(e^{-\beta U_3}-1\right)\right\rangle_{\Omega_1\Omega_2\Omega_3} d\mathbf{r}_2 d\mathbf{r}_3$$

where $f_{kl} = \exp\left(-\beta U_2(kl)\right) - 1$ is the Mayer function for interaction of molecules k and l, and $\beta = 1/k_{\text{B}}T$, with k_{B} Boltzmann's constant. The angle brackets indicate an average over all molecule orientations. The term $B_{ij}^{(\text{pair})}$ is the contribution to the third virial coefficient from the pairwise-additive component of the potential, while $B_{ij}^{(\text{non-pair})}$ corrects this for the non-pairwise 3-body contributions.

Nuclear quantum effects are significant at some of the conditions examined here.

They can be particularly important for H_2O, due to its small moment of inertia. We treated these effects semiclassically, using the quadratic Feynman-Hibbs effective potential.[34] This is implemented by replacing the actual potential with an effective form, which uses an expansion of the potential with respect to the atom positions to capture the effect of the quantum uncertainty in the position of the nuclear centers. Thus, for the pairwise interaction, we have

$$U_2^{\mathrm{QFH}}(T) = U_2 + \frac{\hbar^2}{12 k_{\mathrm{B}} T} \sum\nolimits_i \left[\frac{1}{m_i} \nabla^2_{\mathbf{r}_i} U_2 + \frac{1}{2} \sum\nolimits_k \frac{1}{I_{k,i}} \frac{\partial^2 U_2}{\partial \omega^2_{k,i}} \right] \tag{11}$$

where $\hbar$ is the reduced Planck's constant. The sum is over molecules i, each having mass m_i and moment of inertia with principal components $I_{k,i}$. The operator $\nabla^2_{\mathbf{r}_i}$ is the Laplacian with respect to the center-of-mass position of i, and the k sum is over orientations $\omega_{k,i}$ defined for molecule i in the principal axes of its moment of inertia. These derivatives were evaluated by analytic differentiation of the pair potentials. We did not include nuclear quantum effects in the induction contributions, nor in the 3-body potentials.

Confidence limits for all data calculated in this work were determined by analysis of block averages taken during the MSMC process (1000 blocks distributed between the reference and target simulations). Error bars reported here represent the expanded uncertainty with coverage factor $k = 2$ (approximately 95% confidence interval). Uncertainties are representative of only the stochastic error; in particular,

no attempt is made to estimate or represent contributions to the uncertainty due to inaccuracy in the molecular models underlying the calculations.

All computed values are tabulated in the Supporting Information.

Results and Discussion

We begin with results for the second virial coefficients. Although these have been reported previously, it is worthwhile to examine them here to show that the calculations are implemented correctly, to provide context for the third-virial results, and to present some new comparisons.

Results for B_{20}, the second virial coefficient of CO_2, are given in Figs. 1 and 2. The data and models are in remarkably good agreement, though it should be remembered that GCPM for CO_2 was formulated to fit these data. The Hellmann model, on the other hand, is based primarily on *ab initio* calculations, with a single parameter that was adjusted to improve (already good) comparison to experimental $B_{20}(T)$. The calculations show that the semiclassical correction for nuclear quantum effects is at these conditions negligible on the scale of the variation of the virial coefficient across the temperature range, but it is significant on the scale of the precision and accuracy of the calculations (Fig. 2). We see in fact a discrepancy below 200 K between our semiclassical calculations and those of Hellmann, which is surprising, given that both are based on the same model. We find (shown in figure) agreement for the

classical calculations, so the discrepancy must stem from the semiclassical treatment. Experimental data are not available at these temperatures, so we can not identify preferred results through such a comparison. To help resolve this, we have performed path-integral calculations (not shown) to describe the nuclear quantum effects, and find support for our semiclassical results. Notwithstanding this discrepancy, the comparison between the calculations and experiment demonstrates the feasibility of computing accurate second virial coefficients for a small molecule from first-principles quantum mechanical calculations.

The second virial coefficient for water is shown in Fig. 3. Values computed here are compared to the correlation of Harvey and Lemmon.[14] The values calculated from the CCpol2 pair potential lie slightly above the correlation (which is based on experimental data between roughly 313 K and 1173 K, and on calculations from a lower-quality pair potential[35] above 700 K) at all temperatures studied. Notably, this conclusion is reached at low temperatures only after accounting for nuclear quantum effects. The unmodified CCpol2 potential lies below the correlation at temperatures less than about 500 K, but when the semiclassical correction is applied, B_{02} exceeds the correlation values at all temperatures. This behavior is easier to see in Fig. 4, where the computed values are given as a difference with respect to the correlation. Accuracy limits given with the correlation are presented in this figure, and it is clear

that the semiclassical B_{02} exceeds these. In comparing calculated B_{02}, it should also be noted that the semiclassical approach may not be sufficient to capture all of the nuclear quantum effects at low temperatures; a full path-integral approach appears to be needed for quantitative accuracy below about 350 K.[36] The agreement of GCPM water with experiment is no worse than observed in the CCpol2 potential, which is remarkable given that the second virial coefficient was not used in fitting the GCPM parameters. No explicit quantum corrections are applied for GCPM, as it is assumed that these effects are included implicitly as part of the fitting of the model.

The cross second virial coefficient B_{11} is shown in Fig. 5. The values computed in the present work disagree slightly with those published by Wheatley and Harvey[2] (not shown in figure). It was subsequently discovered that the values reported in Table II of Ref. 2 were not computed using the same fit of the potential that was published in the supplemental data of Ref. 2. Wheatley (personal communication) has provided us with second virial coefficients based on the published potential (which is the one we use as well), and we find perfect agreement between his updated values and our results, as shown in the figure.

There are three sets of experimental data against which we can compare the calculated B_{11}. The first set were compiled by Wheatley and Harvey,[2] based on

experimental vapor-saturation data obtained from several sources. The computed B_{11} is not inconsistent with these data, but the error bars on the experimental results are rather large, at least in comparison to the other data sets, so the comparison is not conclusive. We also have B_{11} values derived from experimental $PVTy$ data by Patel et al.[15] Finally, we have B_{11} values reported by Meyer and Harvey,[3] which are based on new experimental data for the dew point of CO_2-H_2O mixtures. The data from Refs. 15 and 3 are mutually consistent, and are precise enough to uncover some systematic difference from the computed values of B_{11}. The comparison suggests that the CO_2-H_2O potential is a bit too attractive, as the computed values lie below experiment for all but the highest temperature. The discrepancy is well within the estimated uncertainty of B_{11} reported by Wheatley and Harvey, based on uncertainty of the potential, and it is much smaller than the difference from experiment observed[2] in calculated values of B_{11} using an earlier CO_2-H_2O potential.[37]

Results for the GCPM CO_2-H_2O potential are also included in the figure. Values from the model using the simple combining rules (Eq. 8) differ significantly from experiment, indicating that the potential is too repulsive. This led us to adjust the cross parameters as described above, yielding $B_{11}(T)$ values that coincide with experiment over the whole temperature range examined here.

The third virial coefficient for CO_2, B_{30}, is presented in Fig. 6. Perhaps the most

striking feature of the data is the clear demonstration of the importance of the 3-body interactions, an observation made previously by Yu and Schmidt.[29] Nuclear quantum effects, on the other hand, do not appear to be significant at these temperatures. There is very good consistency between the results based on Hellmann's CO_2 pair potential and those from Yu and Schmidt. The agreement of the calculated B_{30} values with experiment is very good for $T > 325$ K, while at lower temperature the models show behavior indicating that intermolecular interactions are too attractive, relative to experiment. We also present results for GCPM CO_2,[20] showing excellent agreement with experiment, which is to be expected, as the model was developed in part to describe $B_{30}(T)$ data. Our results differ slightly but significantly from the values reported by Persson;[20] the model and methods are in principle identical, so we are unsure of the origin of this small discrepancy.

Next, in Fig. 7 we examine data for the H_2O third virial coefficient, B_{03}. The significance of nuclear quantum effects is examined (classical vs. semiclassical) at the 2-body level ($U_3 = 0$), and their effect can be seen at the lowest temperatures examined. The semiclassical correction is applied to the 2-body contribution for all other cases. Again, we see strong evidence for the significance of 3-body effects, which over most of the range changes the sign of the coefficient, switching the overall contribution to the pressure from repulsive to attractive. When non-pairwise

contributions are included, the difference in B_{03} resulting from the different modeling approaches is no worse than the differences observed in the experimental data, except at the lowest temperature examined. Considering this uncertainty, the calculated virial coefficients are in good agreement with experiment. The semi-empirical GCPM again shows remarkable agreement, considering that the virial coefficients were not used in its parameterization. Interestingly, the coefficients formulated using simple polarization and 3-body dispersion, on top of the accurate CCpol2 model, differ markedly from the results from the full CCpol23 model. This may relate to previous observations that polarization is not sufficient to capture 3-body effects. In this regard, the good performance of GCPM must be ascribed to its empirical nature, wherein it captures multibody and nuclear quantum effects for condensed phases via its parameterization.

The cross coefficients B_{21} and B_{12} are presented in Figs. 8 and 9, respectively. Calculated values are compared to experimental data from Patel et al.[15] and Meyer and Harvey.[3] In the latter case, values for B_{12} represent estimates based on a water-dimerization model and various second-order virial coefficients, and thus are not based on experiment; the B_{21} values on the other hand are regressed from experimental data, using these estimated values of B_{12}. One should note that the B_{12} values are about 20 times larger than the B_{21} coefficients, reflecting the stronger in-

teractions exhibited by H_2O molecules in comparison to CO_2 (a result also apparent in comparison of B_{03} to B_{30}). Computed values are presented for the *ab initio* based models, as well as the semi-empirical GCPM formulation. These two independent models give results that are in good mutual agreement, lending credibility to both sets of results. This is important, because the calculations are not in good agreement with the experimental data. Those data are somewhat noisy, and for some temperatures it is possible that they are in agreement with the calculations. Below 300 K however, the difference between experiment and the models is significant, and cannot be ascribed to experimental uncertainty.

Conclusions

The study presented here provides a demonstration of the feasibility, but also the complications, involved in developing and applying a quantitatively accurate, *ab initio* based model for intermolecular interactions. We see in particular the value of examination of virial coefficients as a means to establish the accuracy of the molecular model. It should be noted that any attempt to develop a molecular model by fitting of first-principles calculations will necessarily be biased by the choice and weighting of the configurations used to fit the functional form. In principle, this should not matter, but because the fitted potential is only approximate, its ultimate form will depend on these choices. Thus, it may be possible to develop a fitted poten-

tial that captures the computed data with good accuracy, and perhaps agrees with spectroscopic data characterizing clustering, but fails to describe the temperature-dependent virial coefficients with accuracy commensurate to the precision of the experimental and computational data. The virial coefficients depend on the entire potential surface, and their temperature dependence provides a means to emphasize different parts of the surface when making comparison to experiment. On the other hand, good experimental data can be difficult to obtain, particularly for mixtures, and particularly for coefficients beyond the second. In such circumstances, the ability to compute virial coefficients reliably from first principles can be especially useful. Such a facility can provide a route to accurate prediction of gas-phase properties at conditions of importance to engineering and science applications.

Acknowledgements

This work is supported by the U.S. National Science Foundation (NSF) (Grant No. CHE-1027963). Computational resources were provided by the University at Buffalo Center for Computational Research. Partial contribution of the National Institute of Standards and Technology; not subject to copyright in the United States. We are grateful to Dr. R. A. X. Persson for providing source-code implementations of his GCPM of CO_2. D.A.K. is thankful to John Prausnitz for bringing molecular thermodynamics into the mainstream of chemical engineering, while always stressing

the importance of connecting it to practical applications.

References

1. Li H, Jakobsen JP, Wilhelmsen Ø, Yan J. PVTxy properties of CO_2 mixtures relevant for CO_2 capture, transport and storage: Review of available experimental data and theoretical models. *Applied Energy*. 2011;88:3567–3579.

2. Wheatley RJ, Harvey AH. Intermolecular potential energy surface and second virial coefficients for the water–CO_2 dimer. *J Chem Phys*. 2011;134:134309.

3. Meyer CW, Harvey AH. Dew-point measurements for water in compressed carbon dioxide. *AIChE J*. 2015;DOI: 10.1002/aic.14818.

4. Dennis RA, Harp R. Overview of the U.S. Department of Energy's Office of Fossil Energy Advanced Turbine Program for Coal Based Power Systems with Carbon Capture. In: *Proceedings of ASME Turbo Expo 2007*, vol. 2. New York: ASME Press. 2007; pp. 1093–1104.

5. Figueroa JD, Fout T, Plasynski S, McIlvried H, Srivastava RD. Advances in CO_2 capture technology—The U.S. Department of Energy's Carbon Sequestration Program. *International Journal of Greenhouse Gas Control*. 2008;2:9–20.

6. Harvey AH. Thermodynamic Data to Support High-Temperature Syngas Quench Design: Vapor-Liquid Equilibrium Calculations. *Tech. Rep. EPRI Technical Report 1015542*, EPRI, Palo Alto, CA. 2008.

7. Prausnitz JM, Lichtenthaler RN, Gomes de Azevedo E. *Molecular Thermodynamics of Fluid-Phase Equilibria*. Upper Saddle River, NJ: Prentice-Hall, 3rd ed. 1999.

8. Yang S, Schultz AJ, Kofke DA, Harvey AH. Interpreting Gas-Saturation Vapor-Pressure Measurements Using Virial Coefficients Derived from Molecular Models. *J Chem Eng Data*. 2014;59:3183–3192.

9. Barlow NS, Schultz AJ, Weinstein SJ, Kofke DA. An asymptotically consistent approximant method with application to soft- and hard-sphere fluids. *J Chem Phys*. 2012;137:204102.

10. Barlow NS, Schultz AJ, Kofke DA, Weinstein SJ. Critical isotherms from virial series using asymptotically consistent approximants. *AIChE J*. 2014;60:3336–3349.

11. Moldover MR, McLinden MO. Using ab initio "data" to accurately determine the fourth density virial coefficient of helium. *J Chem Thermodyn*. 2010;42:1193–1203.

12. Shaul KRS, Schultz AJ, Kofke DA, Moldover MR. Semiclassical fifth virial coefficients for improved ab initio helium-4 standards. *Chem Phys Lett*. 2012; 531:11–17.

13. Span R, Wagner W. A new equation of state for carbon dioxide covering the fluid region from the triple-point temperature to 1100 K at pressures up to 800 MPa. *J Phys Chem Ref Data*. 1996;25:1509–1596.

14. Harvey AH, Lemmon EW. Correlation for the second virial coefficient of water. *J Phys Chem Ref Data*. 2004;33:369–376.

15. Patel MR, Holste JC, Hall KR, Eubank PT. Thermophysical properties of gaseous carbon dioxide-water mixtures. *Fluid Phase Equil*. 1987;36:279–299.

16. Benjamin KM, Singh JK, Schultz AJ, Kofke DA. Higher-Order Virial Coefficients of Water Models. *J Phys Chem B*. 2007;111:11463–11473.

17. Paricaud P, Předota M, Chialvo AA, Cummings PT. From dimer to condensed phases at extreme conditions: Accurate predictions of the properties of water by a Gaussian charge polarizable model. *J Chem Phys*. 2005;122:244511.

18. Benjamin KM, Schultz AJ, Kofke DA. Virial Coefficients of Polarizable Water: Applications to Thermodynamic Properties and Molecular Clustering. *J Phys Chem C*. 2007;111:16021–16027.

19. Benjamin KM, Schultz AJ, Kofke DA. Fourth and Fifth Virial Coefficients of Polarizable Water. *J Phys Chem B*. 2009;113:7810–7815.

20. Persson RAX. Gaussian charge polarizable interaction potential for carbon dioxide. *J Chem Phys*. 2011;134:034312.

21. Akin-Ojo O, Szalewicz K. How well can polarization models of pairwise nonadditive forces describe liquid water? *J Chem Phys*. 2013;138:024316.

22. Góra U, Cencek W, Podeszwa R, van der Avoird A, Szalewicz K. Predictions for water clusters from a first-principles two- and three-body force field. *J Chem Phys*. 2014;140:194101.

23. Hellmann R. Ab initio potential energy surface for the carbon dioxide molecule pair and thermophysical properties of dilute carbon dioxide gas. *Chem Phys Lett*. 2014;613:133–138.

24. Oakley MT, Wheatley RJ. Additive and nonadditive models of vapor-liquid equilibrium in CO_2 from first principles. *J Chem Phys*. 2009;130:034110.

25. Axilrod BM, Teller E. Interaction of the van der Waals Type Between Three Atoms. *J Chem Phys*. 1943;11:299–300.

26. Axilrod BM. Triple-Dipole Interaction. I. Theory. *J Chem Phys*. 1951;19:719–724.

27. Gray CG, Gubbins KE. *Theory of Molecular Fluids*. Oxford: Oxford University Press. 1984.

28. Stillinger F. *The Liquid State of Matter: Fluids, Simple and Complex*. New York: North-Holland. 1982.

29. Yu K, Schmidt JR. Many-body effects are essential in a physically motivated CO_2 force field. *J Chem Phys*. 2012;136:034503.

30. Schultz AJ, Kofke DA. Etomica: An object-oriented framework for molecular simulation. *J Comput Chem*. 2015;36:573–583.

31. Benjamin KM, Schultz AJ, Kofke DA. Gas-Phase Molecular Clustering of TIP4P and SPC/E Water Models from Higher-Order Virial Coefficients. *Ind Eng Chem Res*. 2006;45:5566–5573.

32. Singh JK, Kofke DA. Mayer Sampling: Calculation of Cluster Integrals using Free-Energy Perturbation Methods. *Phys Rev Lett*. 2004;92:220601.

33. Schultz AJ, Kofke DA. Quantifying Computational Effort Required for Stochastic Averages. *J Chem Theory Comput*. 2014;10:5229–5234.

34. Feynman RP, Hibbs AR. *Quantum Mechanics and Path Integrals*. New York: McGraw-Hill. 1965.

35. Mas E, Bukowski R, Szalewicz K, Groenenboom G, Wormer P, van der Avoird A. Water pair potential of near spectroscopic accuracy. I. Analysis of potential surface and virial coefficients. *J Chem Phys*. 2000;113:6687–6701.

36. Schenter GK. The development of effective classical potentials and the quantum statistical mechanical second virial coefficient of water. *J Chem Phys*. 2002; 117:6573–6581.

37. Makarewicz J, Ha TK, Bauder A. Potential energy surface and large amplitude motions of the water–carbon dioxide complex. *J Chem Phys*. 1993;99:3694–3699.

38. Patel MR, Joffrion LL, Eubank PT. A Simple Procedure for Estimating Virial-Coefficients From Burnett PVT Data. *AIChE J*. 1988;34:1229–1232.

39. Jaeschke M. Determination of the interaction second virial coefficients for the carbon dioxide-ethane system from refractive index measurements. *Int J Thermophys*. 2004;8:81–95.

40. Holste JC, Hall KR, Eubank PT, Esper G, Watson MQ, Warowny W, Bailey DM, Young JG, Bellomy MT. Experimental (P,V_m,T) for Pure CO_2 Between 220 K and 450 K. *J Chem Thermodyn*. 1987;19:1233–1250.

41. Duschek W, Kleinrahm R, Wagner W. Measurement and Correlation of the (Pressure, Density, Temperature) Relation of Carbon Dioxide. 1. the Homogeneous Gas and Liquid Regions in the Temperature-Range From 217 K to 340 K at Pressures Up to 9 MPa. *J Chem Thermodyn.* 1990;22:827–840.

42. Lemmon EW, McLinden MO, Huber ML. *NIST Reference Fluid Thermodynamic and Transport Properties-REFPROP, NIST Standard Reference Database 23, Version 9.1.* Gaithersburg, MD: National Institute of Standards and Technology. 2013.

43. Eubank PT, Joffrion LL, Patel MR, Warowny W. Experimental Densities and Virial-Coefficients for Steam From 348 to 498 K with Correction for Adsorption Effects. *J Chem Thermodyn.* 1988;20:1009–1034.

44. Warowny W, Eubank PT. Generalized Equations of the Burnett P-V-T Methods for Adsorbing Gases. *Fluid Phase Equil.* 1995;103:77–95.

45. Kell GS, McLaurin G, Whalley E. PVT properties of water VII. Vapour densities of light and heavy water from 150 to 500 °C. *Proc R Soc Lond A.* 1989;425:49–71.

46. Abdulagatov IM, Bazaev AR, Gasanov RK, Ramazanova AE. Measurements of the (p, ρ, T) properties and virial coefficients of pure water, methane, n-hexane,

n-octane, benzene, and of their aqueous mixtures in the supercritical region. *J Chem Thermodyn.* 1996;28:1037–1057.

47. Hill PG, Macmillan RDC. Virial equations for light and heavy water. *Ind Eng Chem Res.* 1988;27:874–882.

48. Hall KR, Eubank PT, Holste JC, Marsh KN. Properties of CO_2-Rich Mixtures: Literature Search and Pure CO_2 Data-Phase I. *Tech. Rep. RR-86*, A Joint Research Report by the Gas Processors Assoc., Tulsa, Oklahoma and the Gas Research Institute, Chicago, Illinois. 1985.

Figure Captions

Figure 1. Second virial coefficient of CO_2, B_{20}. Experimental data (open symbols) are from Patel et al.;[38] Jaeschke[39] (multiplied by 1000 to correct an apparent error in the tabulation); Holste et al.;[40] and Duschek et al.[41] Calculated values (filled symbols and line) are from Hellmann,[23] and the present work using the Hellmann model[23] with and without semiclassical corrections (as indicated), and the GCPM for CO_2 from Persson.[20] Confidence limits are smaller than the symbol sizes for all data, or (for Patel et al., Jaeschke, and Holste et al.) are unknown.

Figure 2. Second virial coefficient of CO_2, B_{20}, presented as a difference from the semiclassical values reported by Hellmann.[23] All data sets are as described in Fig. 1. In addition, the solid line is from the EOS of Span and Wagner[13] as implemented by the REFPROP database,[42] and we also present (labeled $(\Delta B_{20})_{\rm cl}$) our classical calculations differenced with respect to the Hellmann classical results. Error bars indicate expanded uncertainties ($k = 2$) and, for the computed quantities, represent only the stochastic error; confidence limits are not known for data having no error bars.

Figure 3. Second virial coefficient of H_2O, B_{02}. Experimental data (open symbols) are from Eubank et al.,[43] Warowny and Eubank,[44] Kell et al.,[45] and Abdulagatov et al.[46] Calculated values (filled symbols) from the present work are based on the

potential of Góra et al.[22] with and without semiclassical corrections (as indicated), and the GCPM for H_2O from Pericaud et al.[17] The experimentally-based correlation of Harvey and Lemmon[14] is shown with the solid line. Confidence limits are smaller than the symbol sizes for all data, or (for Eubank et al. and Warowny-Eubank) are unknown.

Figure 4. Second virial coefficient of H_2O, B_{02}, presented as a difference from the Harvey-Lemmon[14] correlation. All data sets are as described in Fig. 3. The correlation of Hill and MacMillan[47] is also presented. Segmented lines on either side of zero show the reported ($k = 2$) expanded uncertainties of the Harvey-Lemmon correlation. Where not shown, confidence limits are smaller than the symbol sizes, except for Eubank et al. and Warowny-Eubank, for which the confidence limits are unknown.

Figure 5. Cross second virial coefficient of CO_2-H_2O, B_{11}. Experimental data (open symbols) are from Wheatley and Harvey,[2] Meyer and Harvey,[3] and Patel et al.[15] Calculated values (filled symbols) from the present work are based on the potential of Wheatley and Harvey,[2] with and without the semiclassical correction (as indicated). Points labeled GCPM are from the hybrid GCPM based on the models for CO_2[20] and H_2O[17] with the simple combining rules (Eq. (8)), and the GCPMX points are the same, but using adjusted exp-6 parameters to fit the experimental B_{11}.

Solid line joins the points for the semiclassical Wheatley-Harvey model, as computed by Wheatley (see text). Where not shown, confidence limits are smaller than the symbol sizes.

Figure 6. Third virial coefficient of CO_2, B_{30}. Experimental data (open symbols) are from Patel et al.,[38] Holste et al.,[40] Duschek et al.,[41] and Patel/Hall.[15,48] Solid line is from the EOS of Span and Wagner[13] as implemented by the REFPROP database.[42] Calculated values (filled symbols) from the present work are based on the pair potential of Hellmann.[23] Values based on assumption of pairwise-additivity (U_2 only) are labeled '2-body', and show results with and without the semiclassical correction (as indicated). Results labeled '3-body' include the contribution from U_3 as given by Eqs. (5) and (6), using the semiclassical U_2. Data indicated as Yu and Schmidt are as reported in Ref. 29 and are based on 2- and 3-body models given there. GCPM data are based on the model of Persson[20] as computed in the present work (diamonds), and as reported by Persson (triangles). Where not shown, confidence limits are smaller than the symbol sizes, except for Patel et al., Holste et al., and Duschek et al., for which the confidence limits are unknown.

Figure 7. Third virial coefficient of H_2O, B_{03}. Experimental data (open symbols) are from Eubank et al.,[43] Warowny and Eubank,[44] Kell et al.,[45] and Abdulagatov et al.[46] Calculated values (filled symbols) from the present work are based on the

potential of Góra et al.[22] with and without semiclassical corrections for U_2 (as indicated). Results that include the 3-body contribution U_3 are indicated, using the generic polarization+dispersion approach (Eqs. (5) and (6)), and the full 3-body potential U_3 of Góra et al.[22] GCPM values are computed using the model of Pericaud et al.[17] Where not shown, confidence limits are smaller than the symbol sizes, except for Eubank et al., Warowny-Eubank, and Kell et al., for which the confidence limits are unknown.

Figure 8. Cross third virial coefficient for CO_2-CO_2-H_2O, B_{21}. Experimental data (open symbols) are from Patel et al.[15] and Meyer and Harvey.[3] Calculated values (filled symbols) from the present work are based on the combination of pair and 3-body potentials (Eqs. (5) and (6)) as described in the text. Data labeled GCPM use the hybrid CO_2-H_2O GCPM model with the combining rules given by Eq. (8), and the GCPMX data are the same, but with CO_2-H_2O exp-6 parameters fit to experimental B_{11} data. Where not shown, confidence limits are smaller than the symbol sizes, except for Patel et al., for which the confidence limits are unknown.

Figure 9. Cross third virial coefficient for CO_2-H_2O-H_2O, B_{12}. Data are as described for Fig. 8.

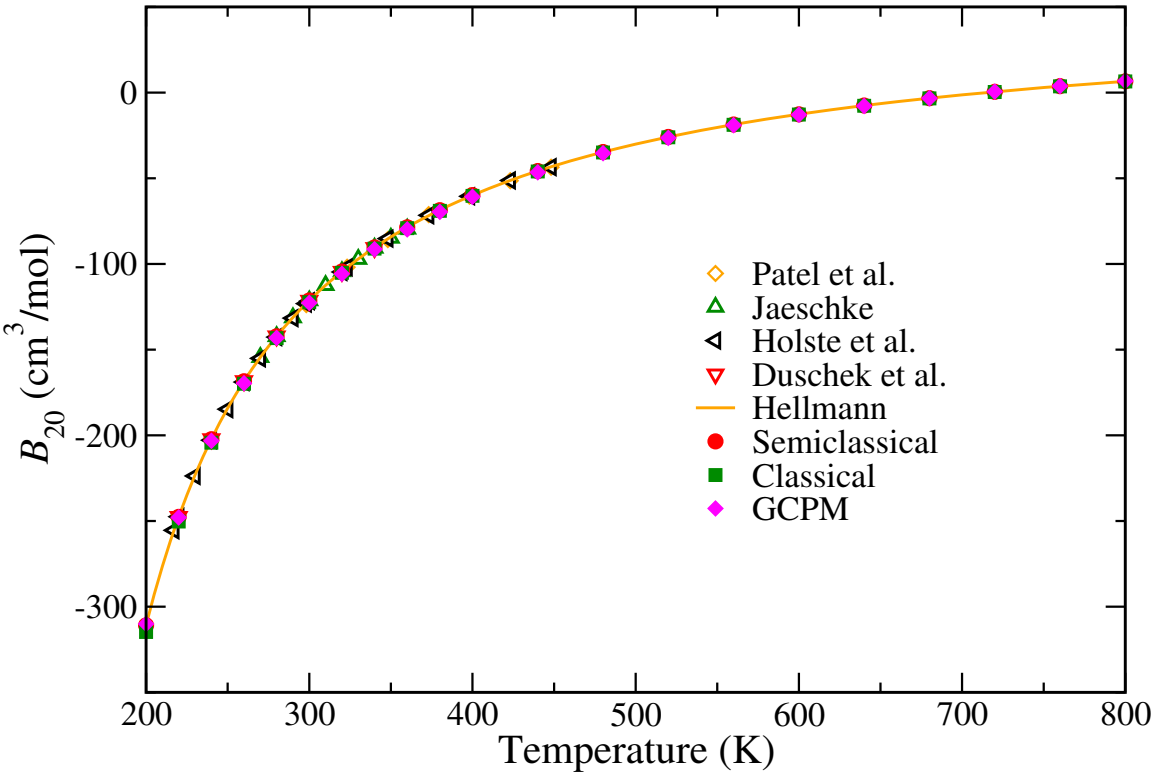

Figure 1: Second virial coefficient of CO_2, B_{20}. Experimental data (open symbols) are from Patel et al.;[38] Jaeschke[39] (multiplied by 1000 to correct an apparent error in the tabulation); Holste et al.;[40] and Duschek et al.[41] Calculated values (filled symbols and line) are from Hellmann,[23] and the present work using the Hellmann model[23] with and without semiclassical corrections (as indicated), and the GCPM for CO_2 from Persson.[20] Confidence limits are smaller than the symbol sizes for all data, or (for Patel et al., Jaeschke, and Holste et al.) are unknown.

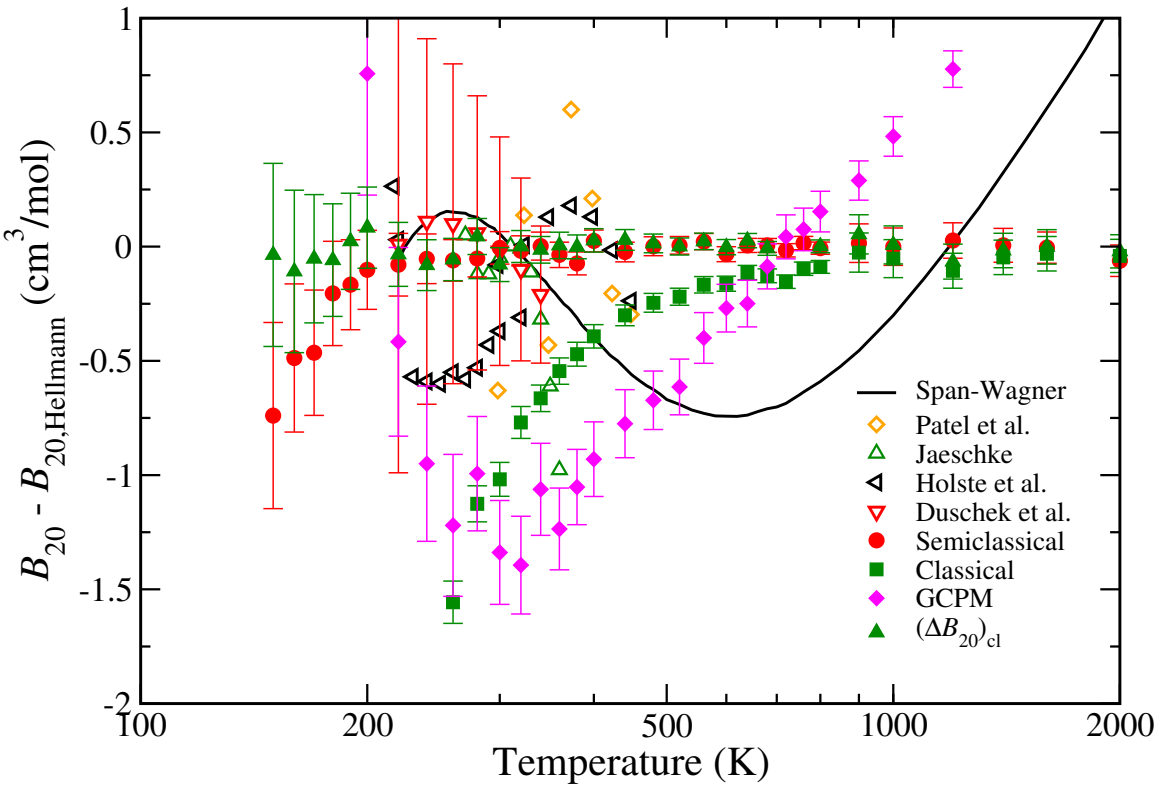

Figure 2: Second virial coefficient of CO_2, B_{20}, presented as a difference from the semiclassical values reported by Hellmann.[23] All data sets are as described in Fig. 1. In addition, the solid line is from the EOS of Span and Wagner[13] as implemented by the REFPROP database,[42] and we also present (labeled $(\Delta B_{20})_{\mathrm{cl}}$) our classical calculations differenced with respect to the Hellmann classical results. Error bars indicate expanded uncertainties ($k = 2$) and, for the computed quantities, represent only the stochastic error; confidence limits are not known for data having no error bars.

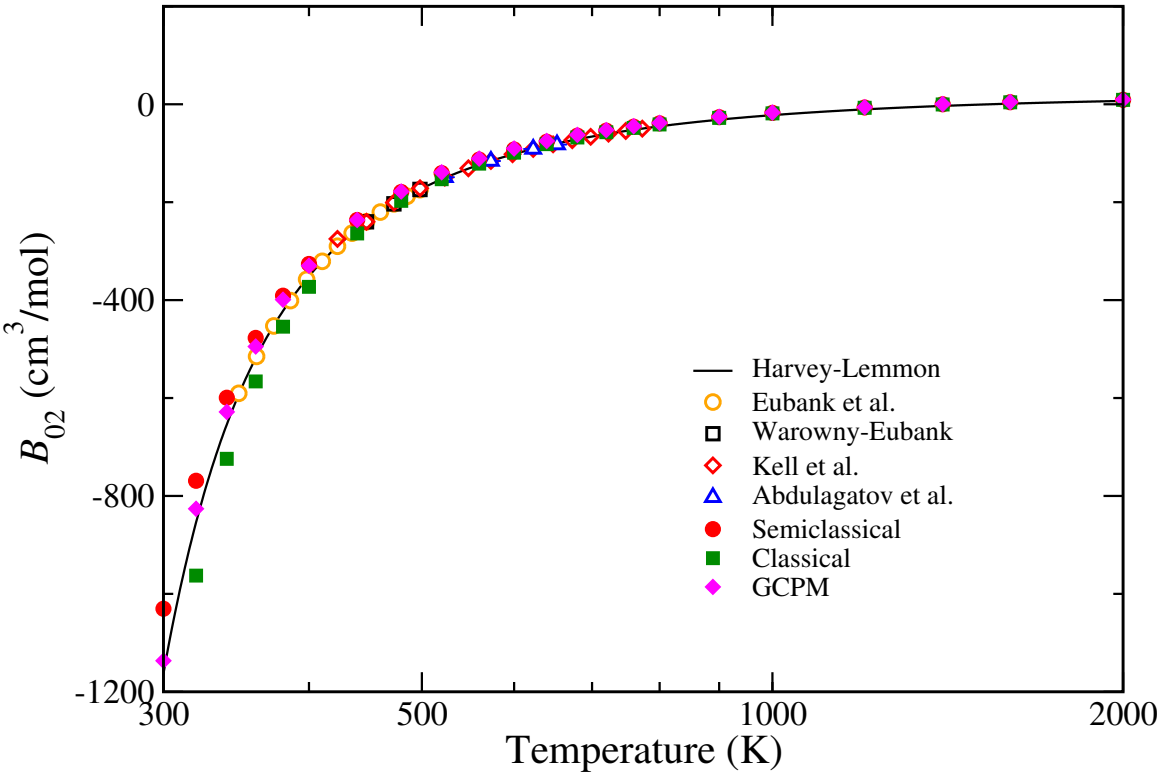

Figure 3: Second virial coefficient of H_2O, B_{02}. Experimental data (open symbols) are from Eubank et al.,[43] Warowny and Eubank,[44] Kell et al.,[45] and Abdulagatov et al.[46] Calculated values (filled symbols) from the present work are based on the potential of Góra et al.[22] with and without semiclassical corrections (as indicated), and the GCPM for H_2O from Pericaud et al.[17] The experimentally-based correlation of Harvey and Lemmon[14] is shown with the solid line. Confidence limits are smaller than the symbol sizes for all data, or (for Eubank et al. and Warowny-Eubank) are unknown.

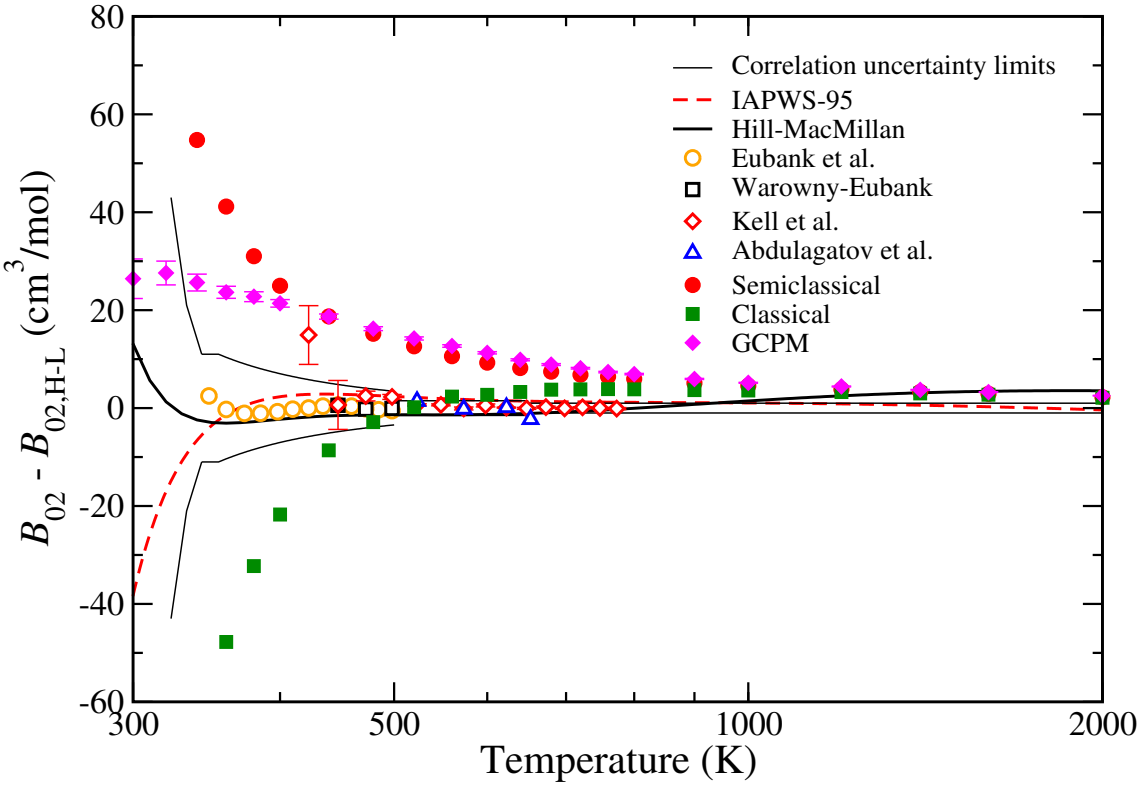

Figure 4: Second virial coefficient of H_2O, B_{02}, presented as a difference from the Harvey-Lemmon[14] correlation. All data sets are as described in Fig. 3. The correlation of Hill and MacMillan[47] is also presented. Segmented lines on either side of zero show the reported ($k = 2$) expanded uncertainties of the Harvey-Lemmon correlation. Where not shown, confidence limits are smaller than the symbol sizes, except for Eubank et al. and Warowny-Eubank, for which the confidence limits are unknown.

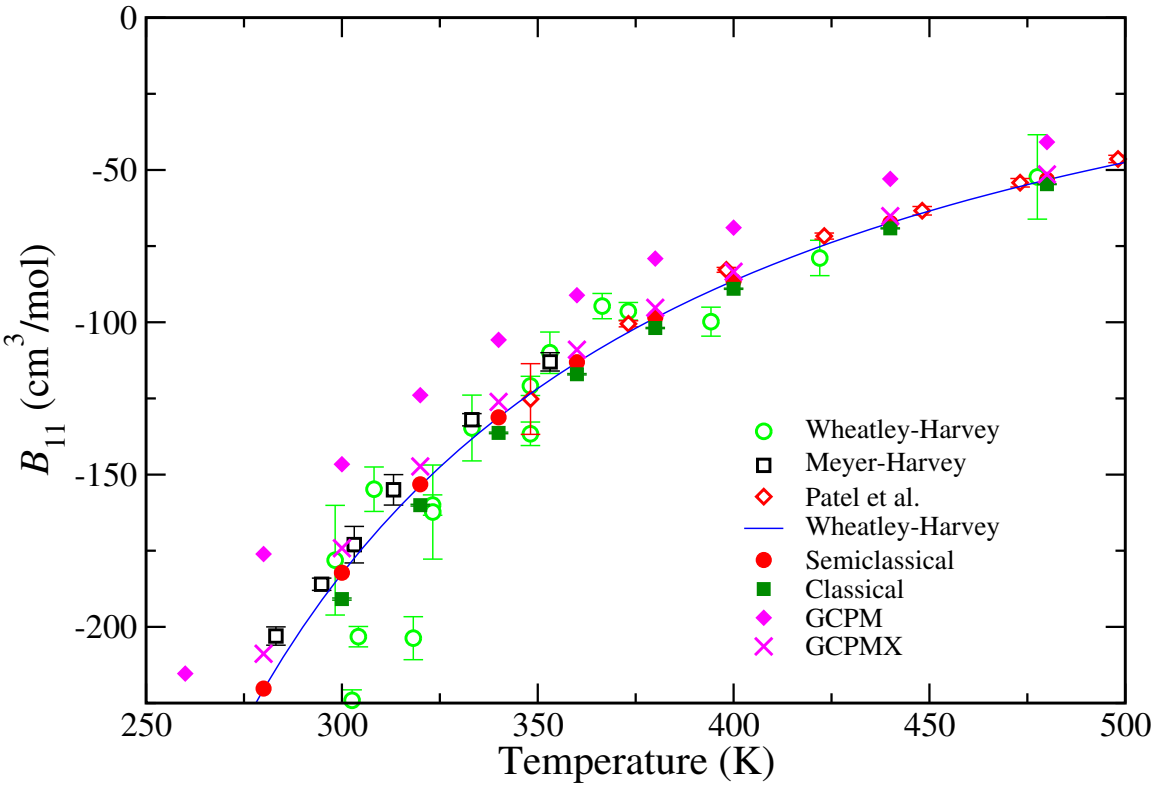

Figure 5: Cross second virial coefficient of CO_2-H_2O, B_{11}. Experimental data (open symbols) are from Wheatley and Harvey,[2] Meyer and Harvey,[3] and Patel et al.[15] Calculated values (filled symbols) from the present work are based on the potential of Wheatley and Harvey,[2] with and without the semiclassical correction (as indicated). Points labeled GCPM are from the hybrid GCPM based on the models for CO_2[20] and H_2O[17] with the simple combining rules (Eq. (8)), and the GCPMX points are the same, but using adjusted exp-6 parameters to fit the experimental B_{11}. Solid line joins the points for the semiclassical Wheatley-Harvey model, as computed by Wheatley (see text). Where not shown, confidence limits are smaller than the symbol sizes.

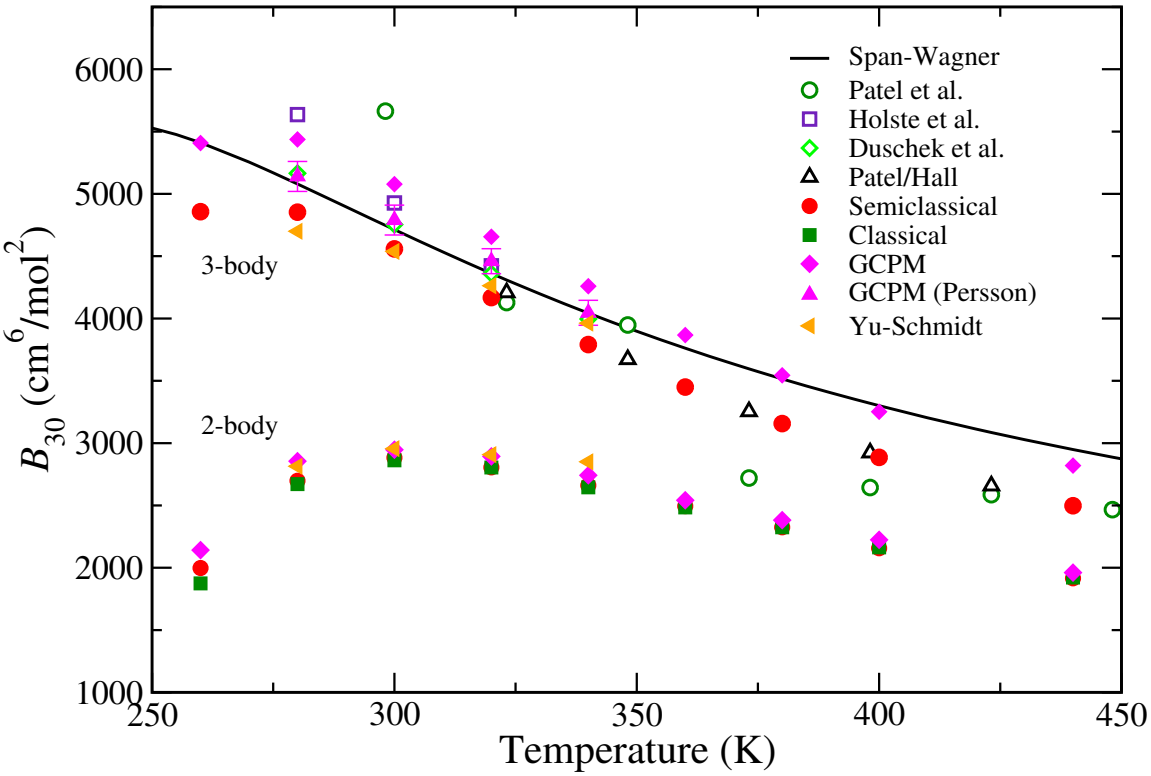

Figure 6: Third virial coefficient of CO_2, B_{30}. Experimental data (open symbols) are from Patel et al.,[38] Holste et al.,[40] Duschek et al.,[41] and Patel/Hall.[15,48] Solid line is from the EOS of Span and Wagner[13] as implemented by the REFPROP database.[42] Calculated values (filled symbols) from the present work are based on the pair potential of Hellmann.[23] Values based on assumption of pairwise-additivity (U_2 only) are labeled '2-body', and show results with and without the semiclassical correction (as indicated). Results labeled '3-body' include the contribution from U_3 as given by Eqs. (5) and (6), using the semiclassical U_2. Data indicated as Yu and Schmidt are as reported in Ref. 29 and are based on 2- and 3-body models given there. GCPM data are based on the model of Persson[20] as computed in the present work (diamonds), and as reported by Persson (triangles). Where not shown, confidence limits are smaller than the symbol sizes, except for Patel et al., Holste et al., and Duschek et al., for which the confidence limits are unknown.

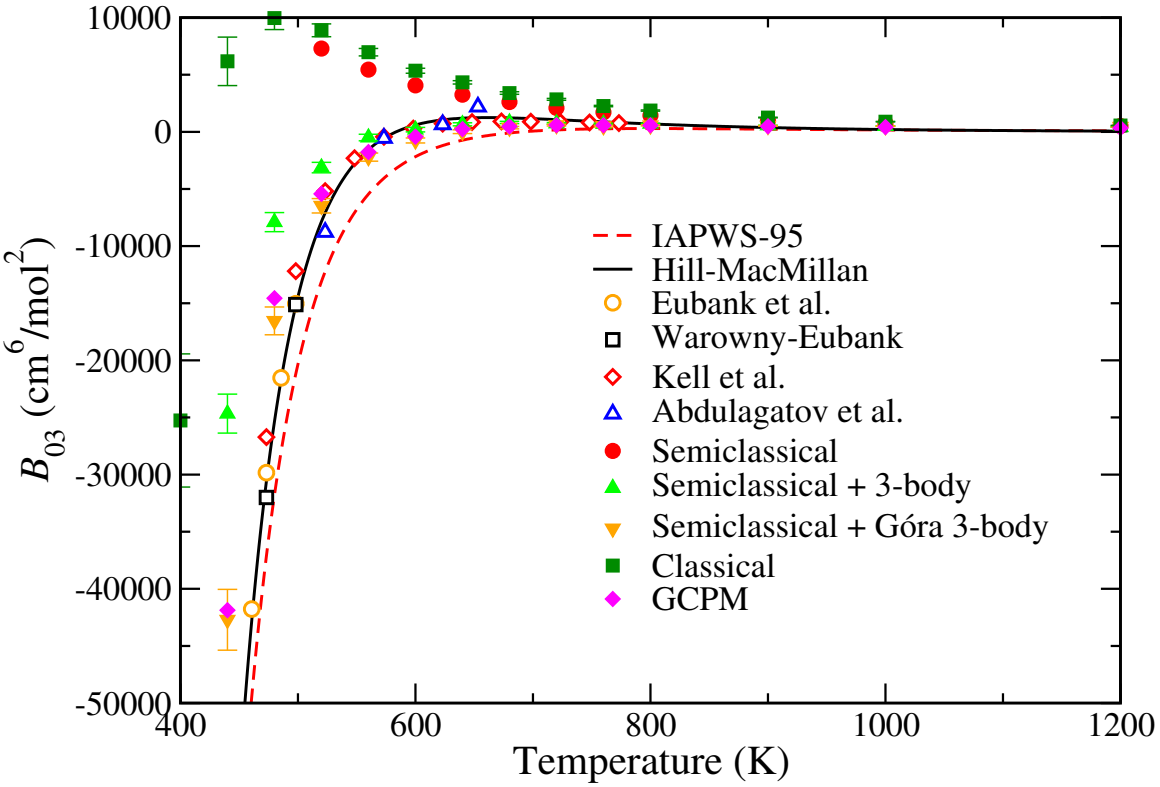

Figure 7: Third virial coefficient of H_2O, B_{03}. Experimental data (open symbols) are from Eubank et al.,[43] Warowny and Eubank,[44] Kell et al.,[45] and Abdulagatov et al.[46] Calculated values (filled symbols) from the present work are based on the potential of Góra et al.[22] with and without semiclassical corrections for U_2 (as indicated). Results that include the 3-body contribution U_3 are indicated, using the generic polarization+dispersion approach (Eqs. (5) and (6)), and the full 3-body potential U_3 of Góra et al.[22] GCPM values are computed using the model of Pericaud et al.[17] Where not shown, confidence limits are smaller than the symbol sizes, except for Eubank et al., Warowny-Eubank, and Kell et al., for which the confidence limits are unknown.

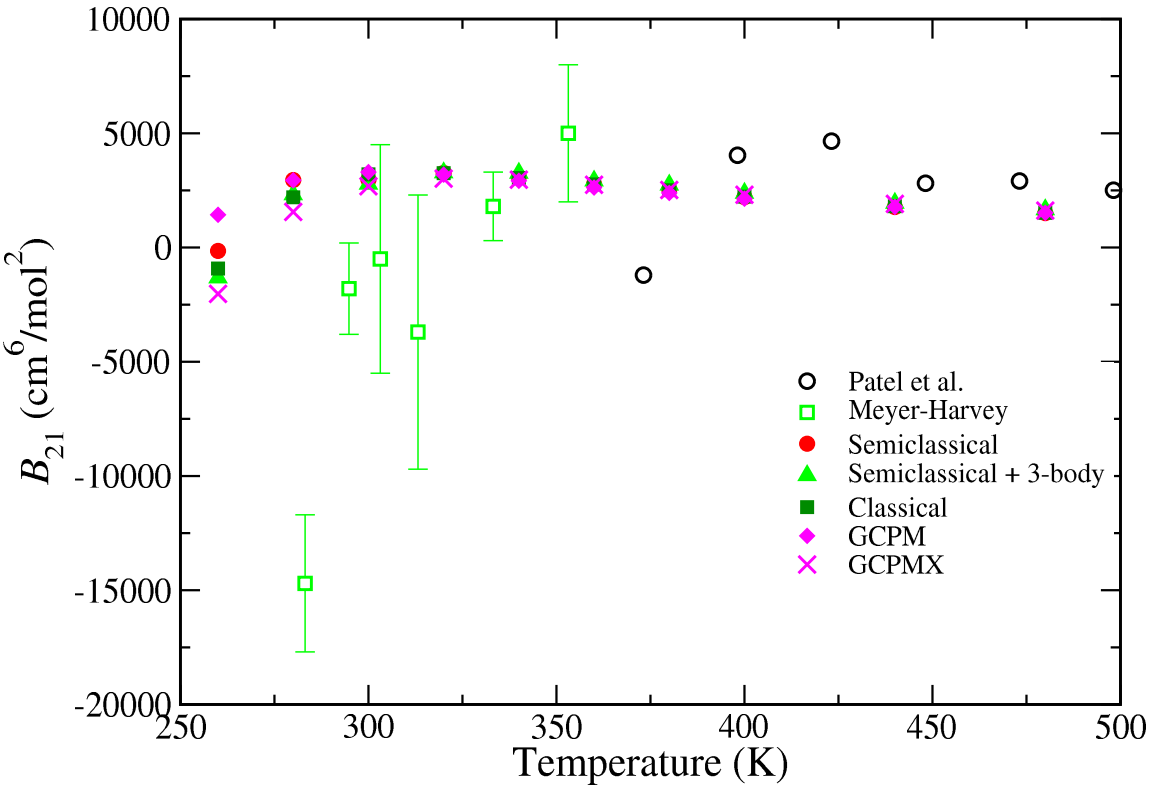

Figure 8: Cross third virial coefficient for CO_2-CO_2-H_2O, B_{21}. Experimental data (open symbols) are from Patel et al.[15] and Meyer and Harvey.[3] Calculated values (filled symbols) from the present work are based on the combination of pair and 3-body potentials (Eqs. (5) and (6)) as described in the text. Data labeled GCPM use the hybrid CO_2-H_2O GCPM model with the combining rules given by Eq. (8), and the GCPMX data are the same, but with CO_2-H_2O exp-6 parameters fit to experimental B_{11} data. Where not shown, confidence limits are smaller than the symbol sizes, except for Patel et al., for which the confidence limits are unknown.

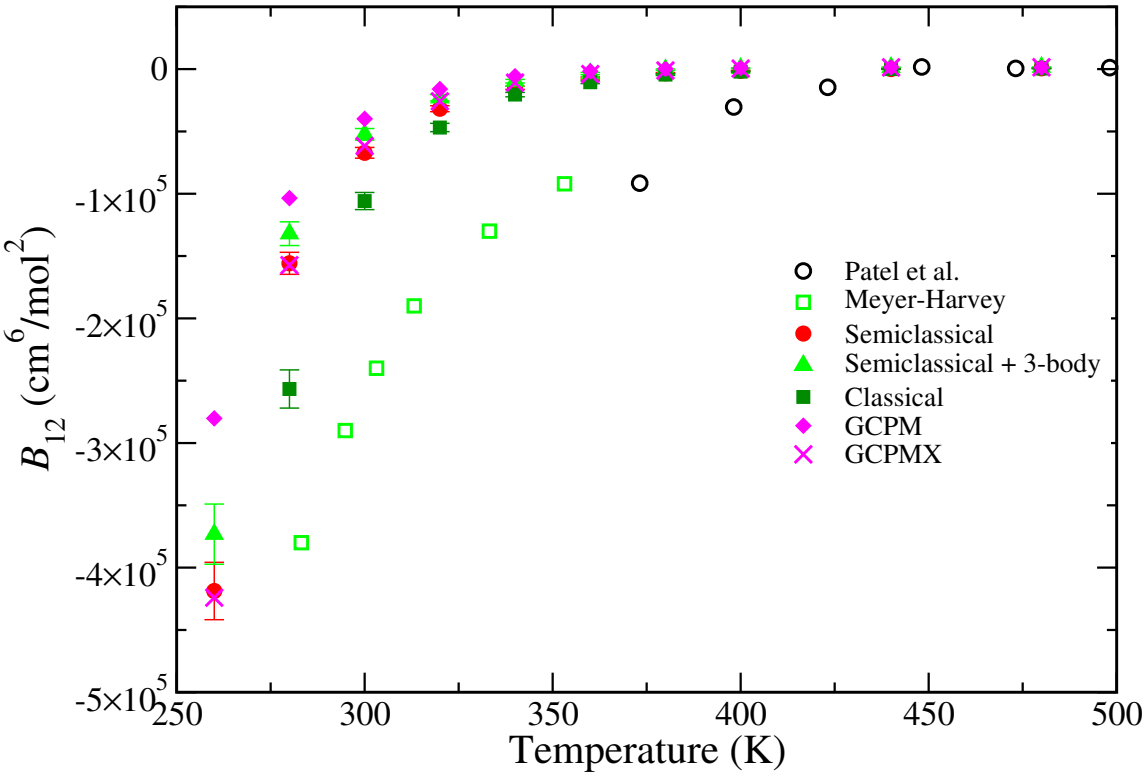

Figure 9: Cross third virial coefficient for CO_2-H_2O-H_2O, B_{12}. Data are as described for Fig. 8.